Erratum

Protein mobilities and P-selectin storage in Weibel–Palade bodies

Nikolai I. Kiskin, Nicola Hellen, Victor Babich, Lindsay Hewlett, Laura Knipe, Matthew J. Hannah and Tom Carter

Journal of Cell Science 123, 3412

doi:10.1242/jcs.080416

There was an error published in the final print and online versions of *J. Cell Sci.* **123**, 2964-2975.

In the legend to Fig. 5, on page 2970, the penultimate sentence incorrectly cites Eqn 4; instead, Eqn 6 should be cited here. The correct sentence should read:

Fluorescence recovery in C was fitted with a decaying exponent $\exp(-t/\tau)$, D=0.15 μm^2/second from Eqn 6, mobile fraction 96.4%.

The Journal apologises for this mistake.

Protein mobilities and P-selectin storage in Weibel–Palade bodies

Nikolai I. Kiskin[1,*], Nicola Hellen[1], Victor Babich[2], Lindsay Hewlett[1], Laura Knipe[1], Matthew J. Hannah[1] and Tom Carter[1,*]

[1]Division of Molecular Neuroendocrinology, MRC National Institute for Medical Research, Mill Hill, London NW7 1AA, UK
[2]CMMCR, UT Southwestern MC, Dallas, TX 75390, USA
*Authors for correspondence (nkiskin@nimr.mrc.ac.uk; tcarter@nimr.mrc.ac.uk)

Accepted 24 May 2010
Journal of Cell Science 123, 2964-2975

doi:10.1242/jcs.073593

Summary

Using fluorescence recovery after photobleaching (FRAP) we measured the mobilities of EGFP-tagged soluble secretory proteins in the endoplasmic reticulum (ER) and in individual Weibel–Palade bodies (WPBs) at early (immature) and late (mature) stages in their biogenesis. Membrane proteins (P-selectin, CD63, Rab27a) were also studied in individual WPBs. In the ER, soluble secretory proteins were mobile; however, following insertion into immature WPBs larger molecules (VWF, Proregion, tPA) and P-selectin became immobilised, whereas small proteins (ssEGFP, eotaxin-3) became less mobile. WPB maturation led to further decreases in mobility of small proteins and CD63. Acute alkalinisation of mature WPBs selectively increased the mobilities of small soluble proteins without affecting larger molecules and the membrane proteins. Disruption of the Proregion–VWF paracrystalline core by prolonged incubation with NH_4Cl rendered P-selectin mobile while VWF remained immobile. FRAP of P-selectin mutants revealed that immobilisation most probably involves steric entrapment of the P-selectin extracellular domain by the Proregion–VWF paracrystal. Significantly, immobilisation contributed to the enrichment of P-selectin in WPBs; a mutation of P-selectin preventing immobilisation led to a failure of enrichment. Together these data shed new light on the transitions that occur for soluble and membrane proteins following their entry and storage into post-Golgi-regulated secretory organelles.

Key words: FRAP, Weibel–Palade bodies, Endothelial cells, Von Willebrand factor, EGFP, Eotaxin-3, P-selectin, Tissue plasminogen activator, Rab27a, CD63

Introduction

The mobility of soluble and membrane proteins in the ER and Golgi complex has been extensively studied (Jackson, 2009; Lippincott-Schwartz et al., 2000; Nagaya et al., 2008; Snapp et al., 2006; Verkman, 2002); however, little is known about protein mobilities within individual regulated secretory organelles (RSOs) (Perez-Vilar et al., 2006). This is because most RSOs are small making direct analysis difficult. Endothelial cells contain large rod-like secretory granules, the Weibel-Palade bodies (WPBs) (Weibel and Palade, 1964). WPB formation is driven by von Willebrand factor (VWF), and their shape is the result of a paracrystalline matrix of tubules composed of the cleaved VWF propolypeptide (Proregion) and mature VWF (Berriman et al., 2009). WPB formation at the trans-Golgi network (TGN) requires a membrane scaffold of AP-1 and clathrin (Lui-Roberts et al., 2005), although in other respects WPB maturation proceeds similarly to other RSOs (Tooze et al., 2001). This includes budding of clathrin-coated vesicles from immature WPBs (Zenner et al., 2007) providing a mechanism for removal of missorted proteins and components not destined for regulated secretion (Arvan and Castle, 1998; Katsumata et al., 2007; Klumperman et al., 1998) and organelle acidification (Erent et al., 2007). Dehydration of organelle content is indicated by a high buoyant density of mature WPBs (Ewenstein et al., 1987) and a membrane tightly apposed to the paracrystalline core (Berriman et al., 2009). WPBs therefore undergo processes common to RSO biogenesis in other cells but uniquely, their size and morphology provide an opportunity to quantitatively analyse protein mobilities in individual RSOs in live cells. An important feature of this secretory system is that immature and mature forms of WPBs can be readily distinguished in living cells by the absence or presence, respectively, of Rab27a (Hannah et al., 2003).

Using fluorescence recovery after photobleaching (FRAP) techniques we determined the diffusional mobility of WPB cargo proteins in the ER, immature and mature WPBs of living cultured human umbilical vein endothelial cells (HUVECs). Because WPBs are only slightly larger than the size of the laser spot used for confocal FRAP, methods were developed to quantify the mobility of proteins in micron-sized rod-like WPBs, using a linear diffusion model and compensating for the ‘corona effect’ (Weiss, 2004). These data reveal the changes in soluble and membrane cargo protein mobilities associated with WPB formation and maturation. We show that alkalinisation of mature WPBs specifically increases the mobilities of small soluble cargo molecules, a process that may contribute to the mechanism underlying their selective release during WPB exocytosis (Babich et al., 2008). The membrane protein P-selectin was immobile in immature and mature WPBs. Disruption of the Proregion–VWF paracrystalline matrix in mature WPBs rendered P-selectin mobile, although VWF remained immobile. Analysis of P-selectin mutants suggests that immobilisation arises from steric entrapment of the large extracellular domain of P-selectin by the immobile paracrystalline matrix of Proregion–VWF tubules, and that immobilisation contributes to retention and enrichment of P-selectin in WPBs.

Results

WPB core proteins are mobile in the ER of HUVECs

To study how the mobilities of soluble proteins change after incorporation into newly-formed WPBs we first determined their mobilities in the ER. Soluble secreted EGFP (ssEGFP, see Materials and Methods) is expressed in the lumen of the ER (supplementary material Fig. S1A); Fig. 1A-D shows a point-FRAP determination of its mobility and distributions of apparent diffusion coefficients D. The distribution of D was broad for ssEGFP, the mean value (Table 1) was close to that estimated in CHO-K1 cells (Dayel et al., 1999). The mean D value for EGFP in the cytoplasm of HUVECs was an order of magnitude higher (Table 1; supplementary material Fig. S2A). The small chemokine eotaxin-3–EGFP was significantly less mobile in the ER than ssEGFP ($P<10^{-4}$; Table 1 and Fig. 1D). Expression of preProVWF–EGFP in HUVECs gives rise to ProVWF–EGFP that exists as a dimer in the ER (Purvis et al., 2007). Its mobility was the slowest (Table 1 and Fig. 1D). We tested if this large heavily glycosylated protein could contribute to molecular crowding and thus slow down ER diffusion of ssEGFP by comparing ssEGFP mobility with that in CHO cells lacking ProVWF. ssEGFP mobilities were the same in both cell types (P=0.19). Coexpression of ProVWF–mRFP did not change D (P=0.31; Table 1) or mobile fractions (P=0.17) of ssEGFP in CHO cells. Thus, ProVWF does not grossly alter the ER environment sensed by ssEGFP in either cell type. The mobility of ProVWF–EGFP in CHO cells was identical to that in the HUVECs (P=0.94), although the mobile fraction was significantly smaller (P=0.001). Proregion–EGFP is much smaller than ProVWF–EGFP, and in the ER (pH 7.2) (Erent et al., 2007) it will not interact strongly with ProVWF (Babich et al., 2009; Hannah et al., 2005). Consistent with this, Proregion–EGFP was significantly more mobile than ProVWF–EGFP ($P<10^{-4}$). Tissue plasminogen activator fused to EGFP (tPA–EGFP) had a similar mobility to Proregion–EGFP (P=0.53; Table 1 and Fig. 1D).

VWF-EGFP and Proregion-EGFP become immobile in immature WPBs and remain immobile in mature WPBs

To distinguish between immature and mature WPBs we coexpressed mRFP–Rab27a with EGFP fusions of core proteins and selected either Rab27a-negative (immature) WPBs in the perinuclear region or Rab27a-positive (mature) WPBs in the cell periphery (supplementary material Fig. S3A,B). Fig. 2 shows FRAP in immature WPBs expressing VWF–EGFP (Fig. 2A) or Proregion–EGFP (Fig. 2B). After bleaching, an abrupt drop in the average fluorescence of the unbleached region, attributed to the 'corona effect' in high-zoom bleaching [see ΔF in supplementary material Fig. S4F and Kumar et al. (Kumar et al., 2010)], was routinely observed. Subsequently, no change in fluorescence in either region occurred over the period of recording showing that both proteins were immobile. Identical results were found in mature WPBs (Fig.

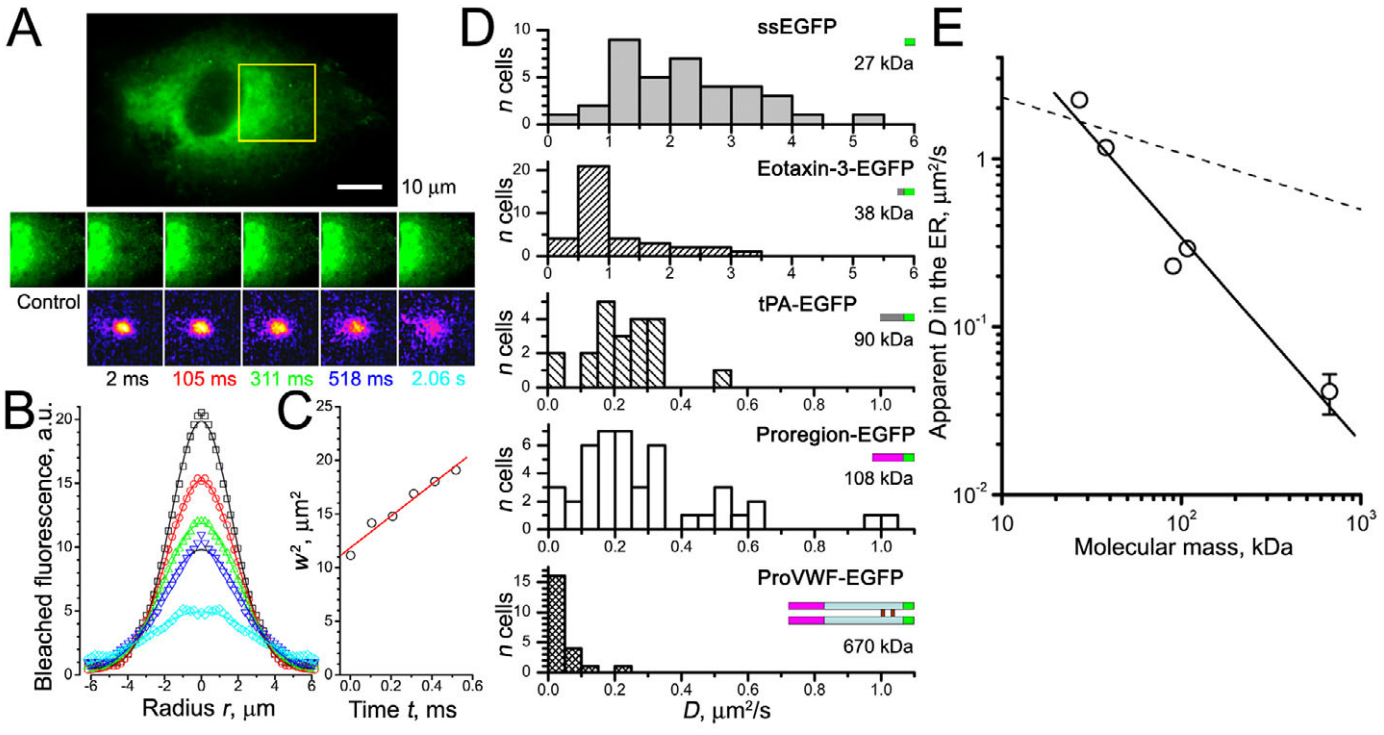

Fig. 1. Point-FRAP method in the ER of HUVECs. (**A**) Top: epifluorescence image of ssEGFP in the ER, scale bar 10 µm. The centre of the region marked in yellow was point-bleached (20 ms, 100% power). Middle row: a prebleach image (control) and images after the bleach at the times indicated. Bottom row: distributions of bleached fluorophore obtained by subtraction of control image and inversion. (**B**) Radial distributions of bleached ssEGFP fluorescence, colour-coded according to the frame times shown in A, smooth lines show Gaussian fits (Eqn 1). (**C**) The squared waist sizes of the Gaussian fits w^2 plotted against time t after bleaching. The red line is a linear fit to these data. From Eqn 2 D=1.8 µm²/second in this experiment. (**D**) Histograms of D values for ssEGFP, eotaxin-3–EGFP, tPA–EGFP, Proregion–EGFP and ProVWF–EGFP. Bin widths 0.5 µm²/second for ssEGFP and eotaxin-3–EGFP, 0.05 µm²/second for other proteins. Cartoons of molecules are shown with approximate molecular masses (EGFP in green). (**E**) Double logarithmic plot of diffusional mobilities of proteins in the ER plotted against their approximate molecular masses (indicated in D). s.e.m. bars are shown where they exceed symbol size. The solid line is the best fit slope, –1.60, the dashed line indicates the Stokes–Einstein theory slope –1/3.

Table 1. Mobilities of WPB cargo proteins measured by FRAP methods

Protein	Cell type	$n_{mobile}/n_{immob.}$ (cells/WPBs)	D[a] ± s.e.m. (μm^2/second)	Mobile fraction (% ± s.e.m.)	$n_{Mob.\ fraction}$ (cells/WPBs)
Cytoplasm					
EGFP	HUVEC	30/0	38±1.0	94±0.85	21
ER					
ssEGFP	HUVEC	36/0	2.2±0.18	87±1.6	20
Eotaxin-3–EGFP	HUVEC	38/0	1.2±0.14	69±3.8	27
tPA–EGFP	HUVEC	21/0	0.23±0.025	70±4.6	17
Proregion–EGFP	HUVEC	44/0	0.29±0.033	87±2.4	41
ProVWF–EGFP	HUVEC	22/0	0.041±0.011	86±4.4	20
ssEGFP	CHO	23/0	2.6±0.25	84±2.7	18
ssEGFP + ProVWF[b]	CHO	18/0	3.0±0.28	89±1.5	16
ProVWF–EGFP	CHO	8/0	0.079±0.050	47±8.3	8
Immature WPBs					
ssEGFP	HUVEC	17/0	0.60±0.15	93±2.2	17
Eotaxin-3–EGFP	HUVEC	24/2	$0.028\pm5.5\times10^{-3}$	77±5.5	25
			$[0.030\pm5.7\times10^{-3}]$[c]	[83±3.4]	[23]
tPA–EGFP	HUVEC	0/3	immobile	–	
Proregion–EGFP	HUVEC	0/17	immobile	–	
VWF–EGFP	HUVEC	0/4	immobile	–	
P-selectin–EGFP	HUVEC	1[d]/18	immobile	–	
EGFP–CD63	HUVEC	20/0	0.24±0.030	91±2.0	20
Mature WPBs					
ssEGFP	HUVEC	26/3	0.15±0.037	81±4.3	29
			[0.17±0.040]	[88±2.0]	[26]
Eotaxin-3–EGFP	HUVEC	11/15	$7.7\times10^{-3}\pm4.1\times10^{-3}$	47±7.1	26
			$[0.018\pm9.0\times10^{-3}]$	[85±3.5]	[15]
tPA–EGFP	HUVEC	0/12	immobile	–	
Proregion–EGFP	HUVEC	0/25	immobile	–	
VWF–EGFP	HUVEC	0/13	immobile	–	
P-selectin–EGFP	HUVEC	0/16	immobile	–	
P-selectin–EGFP	HEK293[e]	5/18	immobile	–	
			[0.024±0.012]	[76±13]	[5]
P-selectin-ΔCT–EGFP	HUVEC	2/18	immobile	–	
			$[1.7\times10^{-3}\pm3.7\times10^{-4}]$	[46±17]	[2]
P-selectin-ΔCT–EGFP	HEK293[e]	3/17	immobile	–	
			[0.014±0.013]	[62±4.9]	[3]
P-selectin-Δ8CCR–EGFP	HUVEC	27/12	$0.037\pm9.2\times10^{-3}$	49±6.0	38
			[0.053±0.012]	[71±3.7]	[26]
P-selectin-Δ8CCR–EGFP	HEK293[e]	37/4	0.052±0.012	60±4.4	39
			[0.058±0.012]	[67±3.3]	[35]
EGFP–CD63	HUVEC	35/0	0.11±0.012	88±2.1	34
EGFP–Rab27a	HUVEC	43/0	0.68±0.045	89±1.9	34
Mature WPBs acutely exposed to NH_4Cl					
ssEGFP	HUVEC	25/0	0.64±0.13	92±1.9	25
Eotaxin-3–EGFP	HUVEC	23/5	0.033±0.011	75±4.0	27
			[0.040±0.014]	[83±2.0]	[23]
tPA–EGFP	HUVEC	1[d]/7	immobile	–	
Proregion–EGFP	HUVEC	0/14	immobile	–	
VWF–EGFP	HUVEC	0/10	immobile	–	
P-selectin–EGFP	HUVEC	0/14	immobile	–	
EGFP–CD63	HUVEC	24/0	0.13±0.013	94±1.8	24
EGFP–Rab27a	HUVEC	23/0	0.71±0.058	94±1.3	23
WPBs rounded by prolonged exposure to NH_4Cl					
P-selectin–EGFP	HUVEC	13/0	0.063±0.021	89±4.4	13
VWF–EGFP	HUVEC	0/7	immobile	–	
Plasma membrane					
Rab35	HUVEC	16/0	0.87±0.080	96±0.99	17

[a] D values calculated for all experiments, immobile cases included as 0 values.
[b] ProVWF–mRFP coexpressed with ssEGFP in CHO cells.
[c] Numbers in square brackets [] apply selectively to mobile cases.
[d] D values did not exceed 0.01 μm^2/second.
[e] Pseudo-WPBs formed in HEK293 cells by coexpression of VWF–mRFP were regarded as 'mature'.

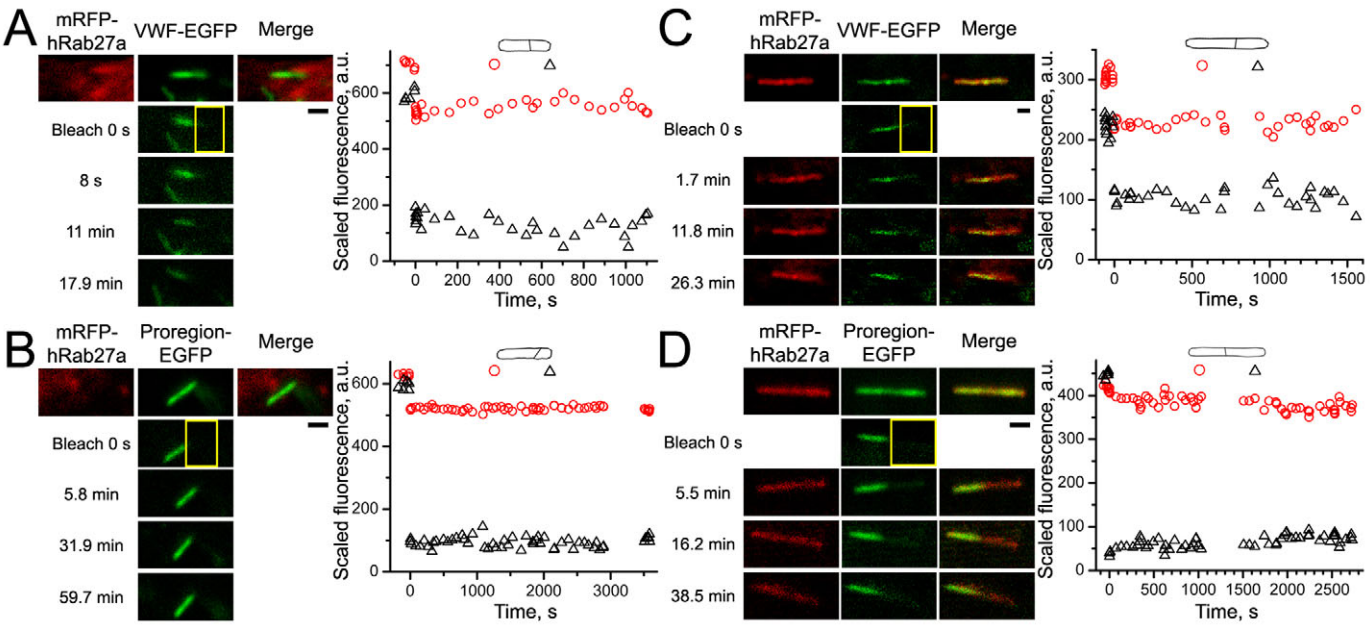

Fig. 2. VWF–EGFP and Proregion–EGFP are immobile in immature and mature WPBs. Leftmost panels in each image series show the absence or presence of mRFP–Rab27a in WPB membranes allowing identification of immature (**A**,**B**) or mature (**C**,**D**) WPBs, respectively. The middle panels show, from top to bottom, a control image, an image of the bleaching frame at t=0 seconds (bleaching ROI is indicated in yellow here and in all subsequent figures) and three postbleach images at the times indicated to the left of images. Rightmost panels in series show mRFP–Rab27a and EGFP–core protein fluorescences superimposed. All scale bars in this and subsequent figures are 1 μm. The graphs here and below show the time courses of average fluorescence, after scaling according to the Eqn 3, recorded in split ROIs (shown schematically above the graphs). Red circles and black triangles indicate the fluorescence in nominally unbleached and bleached ROIs, respectively. a.u., arbitrary units.

2C,D). Although mRFP–Rab27a was also partially bleached during EGFP bleaching, its fluorescence recovered rapidly (see below), allowing the size, shape and location of the WPB to be tracked. tPA–EGFP was also immobile in both immature and mature WPBs (Table 1).

ssEGFP and eotaxin-3–EGFP mobility progressively decreases during WPB formation and maturation

Expressed ssEGFP entered WPBs (supplementary material Fig. S1B). In many immature WPBs ssEGFP fluorescence showed fast recovery after bleaching (Fig. 3A and Table 1), although some had slower recovery, with D values <0.25 μm^2/second (9/17 or 53%). By contrast, ssEGFP mobility in the majority of mature WPBs was significantly slower than in immature WPBs (P<0.001; Fig. 3B and Table 1), with D values typically <0.25 μm^2/second [25/29 or 86%, including n=3 (10%) immobile].

Differences in eotaxin-3–EGFP mobility between immature and mature WPBs were qualitatively similar to those for ssEGFP (Fig. 3D), although eotaxin-3–EGFP was much less mobile (Table 1). In 2/26 (7.7%) immature WPBs no recovery was seen, and the mean mobile fraction, 77%, was significantly lower than for ssEGFP (P<0.05; Table 1). Relative to immature WPBs, a larger fraction of mature WPBs, 15/26 (58%), showed no recovery or very slow recovery that was impossible to quantify, and the mobile fraction was significantly reduced relative to immature WPBs (P<0.01; Table 1). The mean value of D also significantly decreased with WPB maturation (P<10^{-4}; Table 1). Thus, the mobilities of small proteins substantially decreased after inclusion in the WPBs and continued to decrease with WPB maturation.

Acute exposure to NH_4Cl increased the mobility of ssEGFP and eotaxin-3–EGFP in mature WPBs, but other core proteins remained immobile

Acute exposure of cells to the weak base NH_4Cl increases intra-WPB pH from ~5.5 to >7.4 with no detectable change in WPB morphology (Erent et al., 2007). Fig. 3C shows FRAP of ssEGFP in mature WPBs exposed to NH_4Cl. A significant increase in D was detected, with D>0.25 μm^2/second in 14/25 WPBs (56%; Table 1) and none being immobile. The mean D value for ssEGFP was not significantly different from that seen in immature WPBs in control cells (P=0.76).

A similar result was obtained for eotaxin-3–EGFP (Fig. 3D, rightmost panel; Table 1). Immobility or extremely slow recovery was seen in a smaller proportion of WPBs (5/28, 18%). The distribution of eotaxin-3–EGFP mobilities was not different from the result in immature WPBs (P=0.091; Fig. 3D, left panel). VWF–EGFP and Proregion–EGFP remained immobile in mature WPBs exposed to NH_4Cl (Table 1). tPA–EGFP was immobile in 6/7 mature WPBs exposed to NH_4Cl, while one showed slow recovery.

Mobility of EGFP–CD63 and EGFP–Rab27a in WPB membranes

EGFP–CD63-positive WPBs could be readily identified by their distinctive morphology, and this was confirmed by coexpression of EGFP–CD63 with mRFP–Rab27a or the WPB-specific core protein Proregion–mRFP. EGFP–CD63 was mobile in immature WPBs (Fig. 4A and Table 1), but significantly less mobile in mature WPBs (P<10^{-4}; Fig. 4B and Table 1); no evidence of immobile EGFP–CD63 was found.

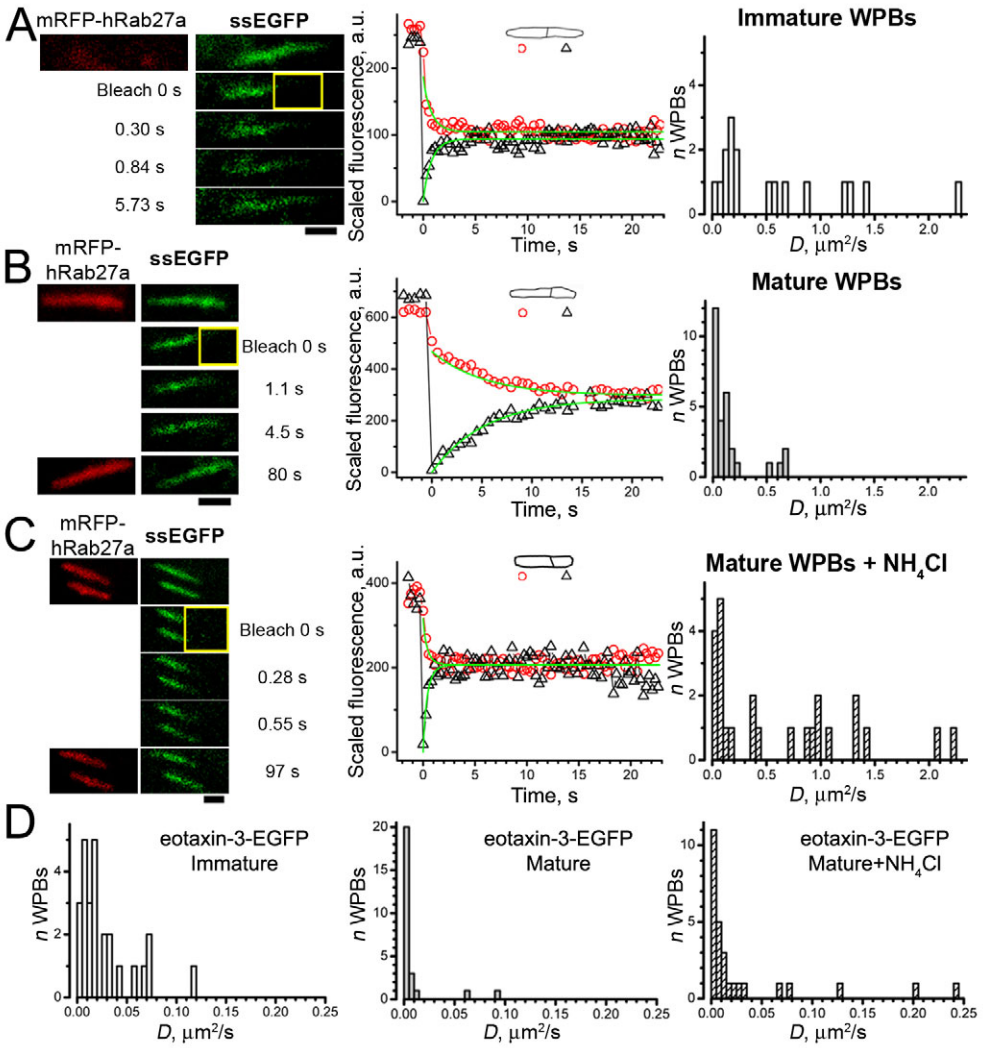

Fig. 3. Formation and maturation of WPBs leads to a progressive decrease in intra-WPB mobility of ssEGFP and eotaxin-3–EGFP, that is reversed in mature WPBs by acute exposure to NH_4Cl. FRAP of (**A**) ssEGFP in an immature mRFP–Rab27a-negative WPB, (**B**) a mature mRFP–Rab27a-positive WPB in a control cell and (**C**) during acute exposure to 40 mM NH_4Cl. (A-C) Left: top images show prebleach images of mRFP–Rab27a fluorescence (left; red) and ssEGFP fluorescence (right; green) in cells coexpressing both constructs; the remaining images show ssEGFP fluorescence in the bleach frame (bleach 0 seconds) and in selected postbleach frames at the times indicated. (B,C) Lower left, images of mRFP–Rab27a fluorescence at the end of the experiment. Middle panels in A-C show plots of the recovery of scaled fluorescence. Smooth lines are fits using the 'corona' diffusion model. For the examples shown, D values were 1.2 μm^2/second (A), D=0.11 μm^2/second (B) and D=1.0 μm^2/second (C). In C the plot is presented for the bottom WPB in the left panel; for the top WPB the value of D was 0.98 μm^2/second. The right panels in A-C show histograms of D values for ssEGFP, ordinates indicate the number of WPBs, bin width 0.05 μm^2/second. (**D**) Histograms of D values for eotaxin-3–EGFP obtained in immature WPBs, mature WPBs and mature WPBs exposed to NH_4Cl, as indicated. Bin width is 0.005 μm^2/second.

EGFP–Rab27a labelled mature WPBs in the cell periphery (supplementary material Fig. S3B). EGFP–Rab27a was the most mobile WPB membrane protein studied, with a broad distribution of D values (Fig. 4D, top right and Table 1). Complete bleaching of EGFP–Rab27a fluorescence in WPBs coexpressing Proregion–mRFP revealed no recovery of EGFP fluorescence over periods of 5–10 minutes (supplementary material Fig. S5, n=5). Acute exposure of mature WPBs to NH_4Cl had no significant effect on the mean D values of the membrane proteins studied (EGFP–CD63, P=0.33; EGFP–Rab27a, P=0.51).

P-selectin–EGFP in WPBs

In all but one case P-selectin–EGFP was immobile in immature WPBs (Fig. 5A, Table 1), as well as in all mature WPBs (Fig. 5B, Fig. 6A, Table 1). Following acute exposure of mature WPBs to NH_4Cl, P-selectin–EGFP remained immobile (n=14, Table 1), however, disruption of WPB morphology by prolonged exposure to NH_4Cl (Michaux et al., 2006a) (supplementary material Fig. S6) rendered P-selectin–EGFP largely mobile, although VWF–EGFP remained immobile (Fig. 5C,D, Table 1).

As in HUVECs, P-selectin–EGFP in pseudo-WPBs of HEK293 cells expressing VWF–mRFP (which lack endogenous P-selectin) was mostly immobile (Fig. 6A, Table 1). A P-selectin mutant lacking the cytoplasmic tail (P-selectin-ΔCT–EGFP) entered WPBs and remained largely immobile, like P-selectin, in both cell types (Fig. 6B). However, deletion of eight of the nine complement consensus repeats (CCR) in the P-selectin extracellular (WPB intralumenal) domain rendered the shorter molecule, P-selectin-Δ8CCR–EGFP, mobile in WPBs of HUVECs and HEK293 cells, although the recovery was often incomplete (Fig. 6C). Neither apparent mobilities nor mobile fractions for this mutant were significantly different in these cell types (Table 1; P=0.12, P=0.30, respectively).

For expressed P-selectin–EGFP (Fig. 7A), as for endogenous P-selectin (Harrison-Lavoie et al., 2006), we found the striking enrichment of protein in membranes of immature WPBs (supplementary material Fig. S3C), quantified by immunofluorescence (see Materials and Methods) as the mean ratio of P-selectin–EGFP content in immature WPBs to that of the adjacent TGN membranes (Fig. 7B). Comparing such ratios in HUVECs expressing the mutants, P-selectin-ΔCT–EGFP and P-selectin-Δ8CCR–EGFP (Fig. 7A) or EGFP–CD63 (not shown), we found that enrichment occurred for immobile but not mobile membrane constructs ($P<10^{-4}$ in pairwise comparsions of mean

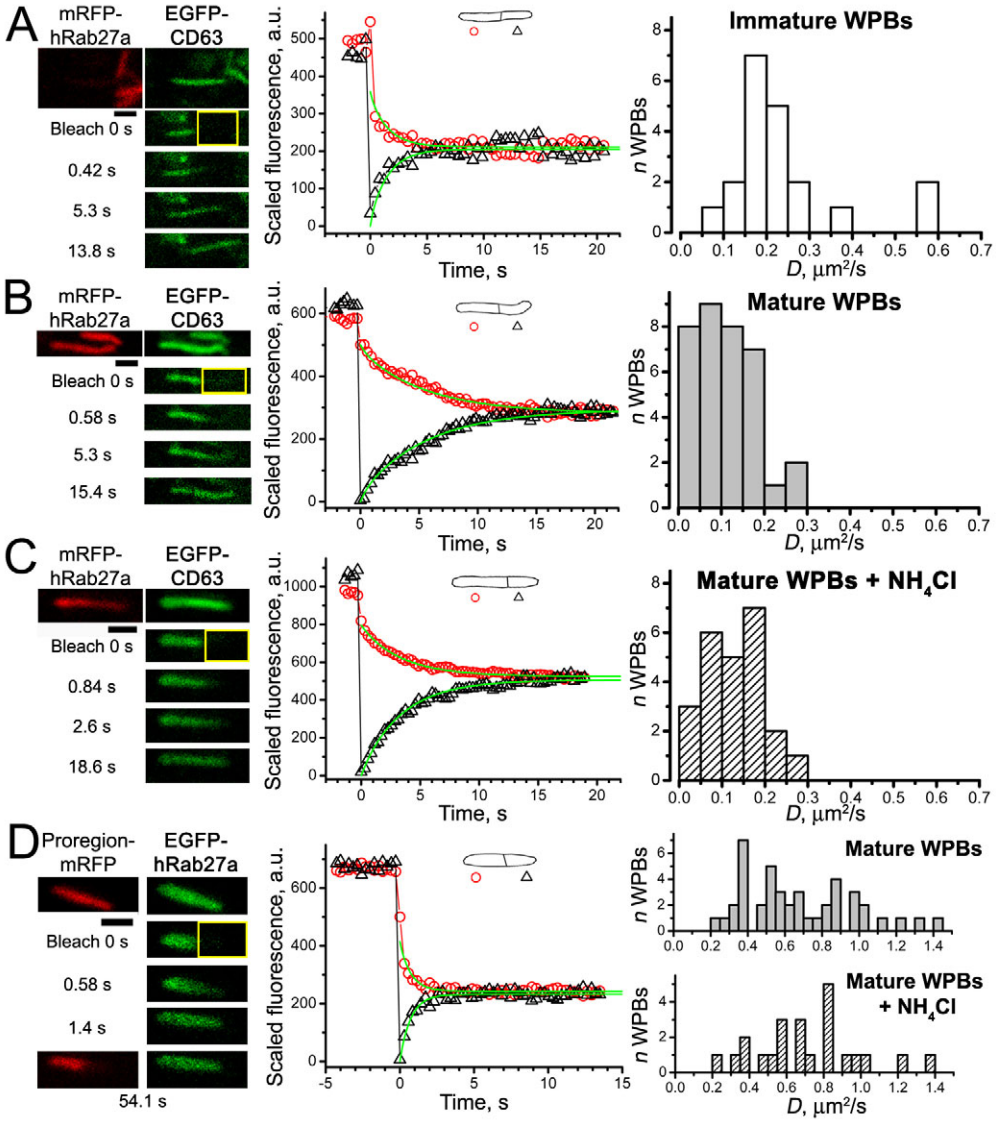

Fig. 4. WPB membrane mobilities of EGFP–CD63 and EGFP–Rab27a; effect of acute exposure of mature WPBs to NH_4Cl. (**A-C**) Left: top images show prebleach images of mRFP–Rab27a and EGFP–CD63 fluorescence; the remaining images show EGFP–CD63 fluorescence in the bleach frame (bleach 0 seconds) and in selected postbleach frames at the times indicated. Middle: graphs showing the time courses of the average fluorescences in WPB ROIs fitted by the model (smooth lines); fitted values of D are 0.38 μm^2/second for immature WPB in (A), 0.16 μm^2/second for mature WPB in (B) and 0.17 μm^2/second for mature WPB in the presence of NH_4Cl (C). Right: histograms of D values obtained in each condition; bin width is 0.05 μm^2/second. (**D**) FRAP of WPB coexpressing EGFP–Rab27a and Proregion–mRFP. EGFP–Rab27a fluorescence recovered quickly after bleaching (middle graph), Proregion–mRFP remained immobile (bottom image). Recovery time course for EGFP–Rab27a is fitted by the model (smooth lines); D=0.57 μm^2/second. Right panels, histograms of D values for EGFP–Rab27a in control (top) and in the presence of NH_4Cl (bottom); bin width 0.05 μm^2/second.

ratios between P-selectin-Δ8CCR–EGFP or EGFP–CD63 and P-selectin or P-selectin-ΔCT–EGFP; Fig. 7B).

Discussion

Soluble WPB cargo is freely mobile in the ER

To characterise the diffusional properties of proteins within the secretory pathway of HUVECs we used EGFP, a probe widely used for determining mobilities in the ER and a range of subcellular compartments in other cells (Dayel et al., 1999; Dross et al., 2009; Kao et al., 1993; Partikian et al., 1998; Swaminathan et al., 1997; Yokoe and Meyer, 1996). High mobilities of EGFP in cytoplasm and ssEGFP in the ER lumen (Table 1) suggest its unobstructed diffusion, as reported in other cells (Dayel et al., 1999; Swaminathan et al., 1997; Yokoe and Meyer, 1996). ProVWF, which exists predominantly as a dimer in the ER, is a very large and heavily glycosylated protein that could increase molecular crowding in the ER, slow down ssEGFP diffusion and produce cell stress (Ellgaard and Helenius, 2003), which reduces the mobile fractions of ER-trafficked proteins (Nagaya et al., 2008). However, ProVWF–mRFP co-expressed with ssEGFP in CHO cells did not significantly alter the apparent ER mobility (P=0.31; Table 1) or mobile fraction (P=0.17) of ssEGFP, indicating that the presence of ProVWF per se does not grossly alter the ER environment sensed by ssEGFP in either cell type. Although a reduction in mobile fraction for Pro-VWF–EGFP might indicate ER stress in CHO cells, in HUVECs the mobile fraction was higher (P=0.001; Table 1), and comparable to other soluble proteins studied. Eotaxin-3–EGFP (~38 kDa) was significantly ($P<10^{-4}$) less mobile than ssEGFP (~27 kDa) in HUVEC ER. For globular proteins the Stokes–Einstein formula predicts a ratio of D values inversely proportional to the cubic root of the ratio of molecular masses (Dross et al., 2009). Eotaxin-3–EGFP and ssEGFP are not true globular proteins, so the ratio of mean D values (~2) exceeded that expected for globular molecules of these sizes. Specific molecular shapes of the two molecules or weak interactions between eotaxin-3–EGFP and other ER components may account for the slower eotaxin-3 mobility. Strong interactions of this protein with endogenous ProVWF seem unlikely because eotaxin-3 does not associate with VWF or Proregion under neutral conditions (pH 7.4) (Babich et al., 2009), similar to those that exist in the HUVEC

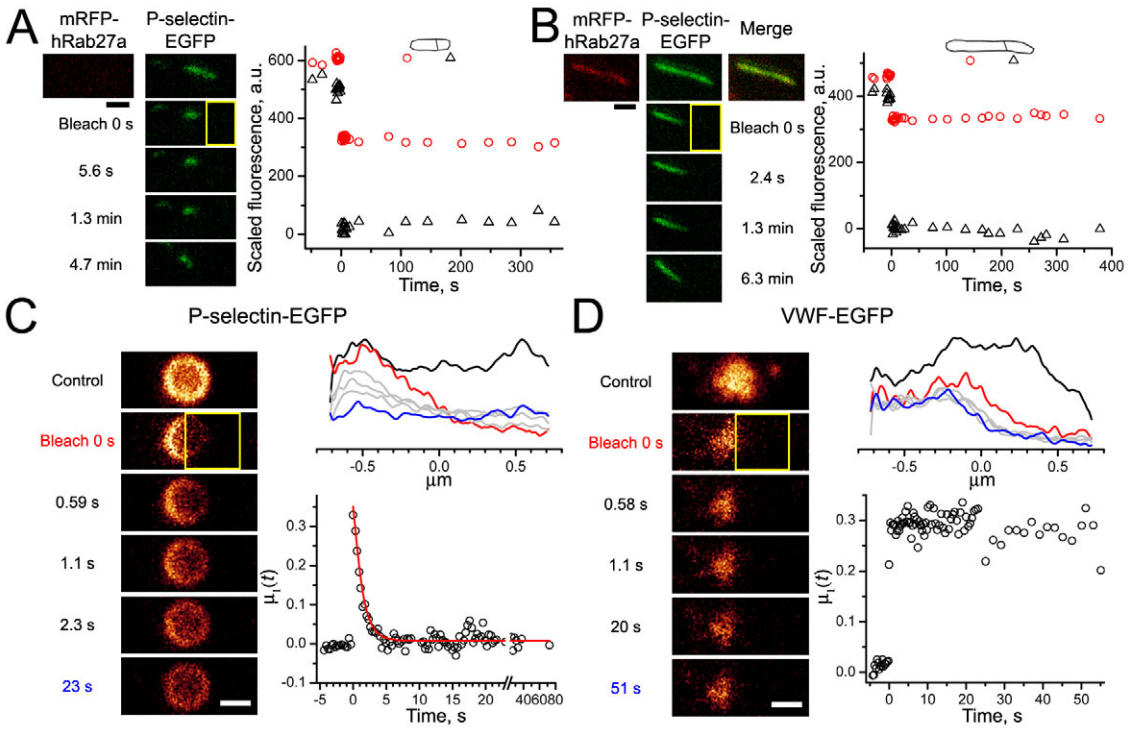

Fig. 5. Mobility of P-selectin–EGFP in intact and disrupted WPBs. (**A**,**B**) Representative experiment on an immature WPB lacking mRFP–Rab27a (A) and a mature mRFP–Rab27a-positive WPB (B). Top panels show prebleach images of mRFP–Rab27a fluorescence (left; red) and P-selectin–EGFP fluorescence (middle panels; green) in cells coexpressing both constructs. The bleaching ROIs are shown in yellow. Right panels show the time courses of the average fluorescence recorded in the split ROIs plotted as in Figs 2–4. (**C**,**D**) Representative FRAP experiments on mature WPBs containing P-selectin–EGFP (C) or VWF–EGFP (D) after morphological collapse induced by prolonged exposure to NH_4Cl. (C,D) Top right panels: the average fluorescence profiles of the rounded WPBs (as shown in left images) before bleaching (black trace), during bleaching (red), on recovery (grey; last time point blue). Bottom right panels show the time course for fluorescence recovery, the ratio of moments $\mu_1(t)$. Fluorescence recovery in C was fitted with a decaying exponent $\exp(-t/\tau)$, D=0.15 μm^2/second from Eqn 4, mobile fraction 96.4%. No recovery of fluorescence was seen for VWF–EGFP (D).

ER (pH 7.2) (Erent et al., 2007). Large differences in apparent D of ProVWF–EGFP relative to ssEGFP alone (~50-fold) is unlikely to be due entirely to their different molecular masses (the predicted ratio of D assuming globular shapes is ~3), but rather to other factors such as the highly prolate molecular shape of soluble ProVWF (Singh et al., 2006) or interactions of ProVWF–EGFP with ER-resident components, possibly through its extensive sugar modifications. In common with the size dependences of mobilities in other cellular compartments (Dross et al., 2009; Lukacs et al., 2000; Papadopoulos et al., 2000; Seksek et al., 1997), the diffusion of soluble secretory proteins within the ER of HUVECs slowed sharply with increased protein size: the dependence of D on approximate molecular mass had a –1.6 logarithmic slope instead of the –0.33 slope predicted by the Stokes–Einstein formula (Fig. 1E).

From ER to the immature WPBs

pH-dependent aggregation of Proregion and VWF into helical tubules is a crucial step in WPB formation. Micron-sized immature WPBs at the TGN contain loosely arranged tubules enclosed by a baggy membrane with clathrin-coated buds (Lui-Roberts et al., 2005; Valentijn et al., 2008; Zenner et al., 2007). The immobility of VWF–EGFP and Proregion–EGFP in immature WPBs indicates that these proteins are completely incorporated into the core tubule structures at early stages before WPB maturation.

Overexpression of ssEGFP or eotaxin-3–EGFP in the HUVEC secretory pathway led to their incorporation into immature WPBs where they remained mobile, although substantially less than in the ER (Table 1). In immature WPBs the apparent D for eotaxin-3–EGFP was an order of magnitude lower than for ssEGFP, with a significantly lower mobile fraction of 77% (P=0.023), showing that its diffusion becomes more restricted with an emergence of the tubular core structure, either because of its larger size compared with ssEGFP or because of more prominent interactions with core components.

Immature RSOs are thought to lose non-aggregated soluble cargo not destined for storage and secretion by segregation to a mobile phase, followed by removal through clathrin-dependent vesicle budding (Arvan and Castle, 1998). The magnitude of mobilities in immature WPBs shows that small soluble non-aggregating molecules should be available for such removal, since on the size scale of a WPB (L=2 μm) even slowly mobile molecules such as eotaxin-3–EGFP have a mean diffusion time $L^2/2D$ of ~1.2 minutes; sufficient for their removal. Clathrin-dependent vesicle budding is restricted to early stages of WPB formation at the TGN and does not continue in mature WPBs (Lui-Roberts et al., 2005; Valentijn et al., 2008; Zenner et al., 2007). The very presence of mobile ssEGFP in mature WPBs suggests that the capacity of the removal mechanisms is limited either by the kinetics or magnitude of vesicle budding processes or the accessibility of mobile material

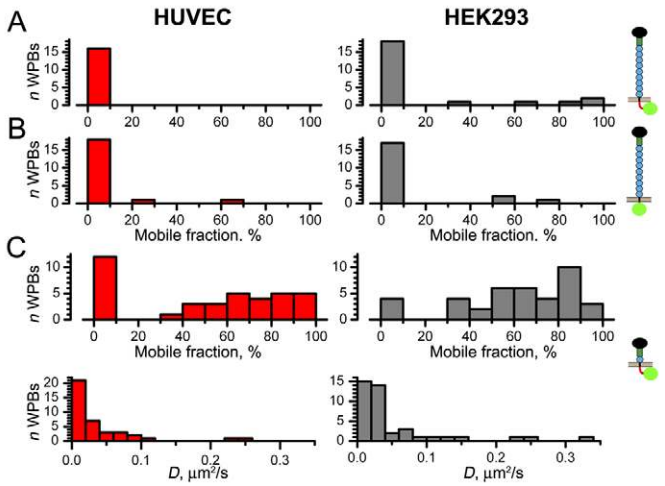

Fig. 6. Mobility of P-selectin–EGFP and P-selectin mutants in WPBs of HUVEC and pseudo-WPBs of HEK293 cells coexpressing VWF–mRFP. (**A-C**) Histograms of the percentage mobile fraction for P-selectin–EGFP (A), P-selectin-ΔCT–EGFP (B) or P-selectin-Δ8CCR–EGFP (C, upper panels) in mature WPBs of HUVECs (left; red) and pseudo-WPBs of HEK293 cells (right; grey). Cartoons indicating the constructs are shown on the right, with EGFP in green. (C) Lower panels show the distributions of apparent diffusion coefficients *D* for P-selectin-Δ8CCR–EGFP, bin width 0.02 μm²/second.

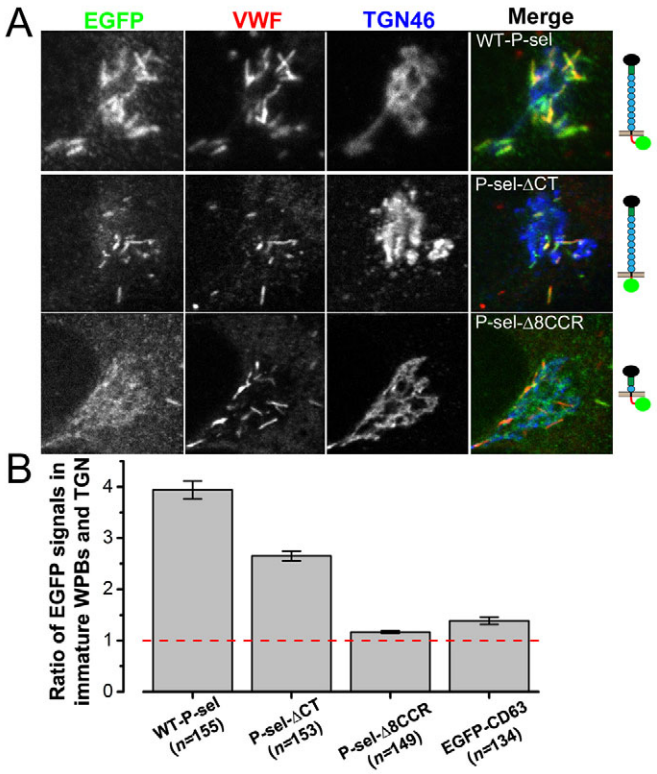

Fig. 7. Immobile but not mobile P-selectin mutants become enriched in immature WPBs. (**A**) Fluorescence images of the Golgi region of fixed immunostained HUVECs expressing (top to bottom) wild-type P-selectin–EGFP, P-selectin-ΔCT–EGFP and P-selectin-Δ8CCR–EGFP; see molecule cartoons on the right. Cells were stained with fluorescent antibodies (from left to right) to EGFP (green in merged images), VWF (red in merged images) and TGN46 (blue in merged images). (**B**) The average ratios of EGFP immunofluorescence from perinuclear WPBs to that of adjacent membranes within the TGN (as described in Data analysis in the Materials and Methods) for these proteins and EGFP–CD63 are plotted. Bars show the s.e.m. Numbers of WPBs measured are shown in parentheses.

within the WPB (see below). Thus following cessation of vesicle budding the core composition of the mature organelle is likely to remain stable until exocytosis.

Decreased mobility of small cargo proteins in mature WPBs and its reversal by NH_4Cl

Ultrastructural comparison of immature and mature WPBs shows an increased electron density following maturation (Zenner et al., 2007). Electron tomography of mature WPBs in vitrified HUVECs shows that the lumen comprises a paracrystalline packing of Proregion-VWF tubules (Berriman et al., 2009). Paracrystal formation is linked to acidification and dehydration of the WPBs, and possible direct interactions between tubules and the membrane. VWF–EGFP and Proregion–EGFP remained immobile in mature WPBs, consistent with their complete incorporation into the paracyrstal.

In mature WPBs ssEGFP and eotaxin-3–EGFP had narrower distributions of apparent mobilities (Fig. 3), lower mean *D* values and decreased mobile fractions (Table 1). The reasons for these are likely to be complex. Dehydration of the organelle could increase the viscosity of the mobile phase and cause it to shrink. Tight packing of tubules in the paracrystal could introduce a ‘molecular sieve’ effect (Papadopoulos et al., 2000) introducing a size dependence for protein diffusion. The largest density gaps in the WPB lumen are the interiors of the tubules themselves (inner diameter of ~12 nm), and the 4–8 nm spaces between the tubules (Berriman et al., 2009). Lateral fenestrations of ~7 nm in the tubule walls may connect tubule interiors (Berriman et al., 2009), providing a route for percolative diffusion of small molecules. Near the percolation threshold, diffusion decreases steeply with the decrease in free WPB volume and increased size of diffusing molecules (Novak et al., 2009), so small decreases in free volume may cause dramatic mobility changes. A similar approx. fourfold reduction in mobilities of ssEGFP and eotaxin3–EGFP with WPB maturation could thus reflect the decrease in free volume with tighter packing of Poregion-VWF tubules and closer apposition of the limiting membrane. Restricted lateral diffusion via tubule fenestrations could result in small soluble molecules being trapped in or between tubules, preventing access to peripheral membrane budding and contributing to their retention. Complete immobility of the larger protein tPA–EGFP is compatible with entrapment, although specific interactions with other cargo components cannot be excluded.

The distributions of *D* for ssEGFP and eotaxin-3–EGFP were similar in immature WPBs and in mature WPBs acutely exposed to NH_4Cl, although the fraction of lower mobilities was still prominent. The retention of the rod-like morphology and immobility of Proregion and VWF in WPBs exposed to NH_4Cl suggest that the matrix of Proregion-VWF tubules within the WPB remained essentially intact. Intra-WPB alkalinisation by NH_4Cl is due to the permeation of NH_3 (Erent et al., 2007; Roos and Boron, 1981); WPB swelling may occur because of influx of water and/or ions that compensate for a slow intra-WPB accumulation of NH_4^+ ions, as shown for lysosomes (Poole and Ohkuma, 1981). Thus, mobility changes seen with NH_4Cl may arise from the reversal of maturation-

and pH-dependent changes in intra-WPB charge or structure, leading to a loosening of the paracrystalline core, from decreased viscosity, or from WPB swelling. As we detected the changes shortly after NH_4Cl addition, a direct pH action seems more likely. In either case, alkalinisation causes reappearance of the mobile phase, although whether its structural features are the same as in immature WPBs, remains to be established.

Increased immobilisation of small cargo during WPB maturation will promote protein retention within the stabilised mature organelle. During WPB exocytosis intra-WPB pH rises, and the organelle hydrates (Erent et al., 2007). The reversible effect of pH on mobilities of small stored molecules would contribute, together with the formation of a fusion pore of restricted dimensions, to the regulation of their selective release during transient or lingering kiss fusion events (Babich et al., 2009; Babich et al., 2008).

Differential changes in membrane protein mobilities during WPB maturation

RSO maturation involves remodelling of the organelle membrane (Katsumata et al., 2007; Zenner et al., 2007) to form a unique membrane composition (Hannah et al., 2002). CD63 molecules are deeply embedded within membranes (Hemler, 2005), so their mobility would rather depend on local membrane properties. The reduced mobility of EGFP–CD63 in mature WPBs may therefore reflect changes in membrane composition after maturation (Katsumata et al., 2007). Alternatively, it could reflect CD63 oligomerisation, weak binding or steric interactions with cytosolic or WPB core elements (Hemler, 2005; Pols and Klumperman, 2009).

Recruitment of Rab27a to mature WPBs is thought to reflect the establishment of a distinct membrane composition (Hannah et al., 2003). Whole WPB bleaching confirmed that fast recovery of EGFP–Rab27a fluorescence in FRAP was exclusively due to redistribution of molecules within the WPB membrane, and not recruitment of non-bleached cytoplasmic EGFP–Rab27a. Rab27a associates with its target membranes through a C-terminal lipid modification (Pereira-Leal et al., 2001), and its mobility will therefore strongly depend on membrane properties. Interestingly, EGFP–Rab27a mobility was lower than that of plasma membrane Rab35 (P=0.029, Table 1; supplementary material Fig. S2B), which is predicted to have the same lipid modification. This may reflect distinct membrane microenvironments or differences in the nature of interactions between these Rabs and their effectors. NH_4Cl did not change EGFP–Rab27a mobility indicating that the properties of the WPB membrane or interactions with Rab27a effectors were not significantly dependent on pH .

P-selectin–EGFP immobilisation in WPBs requires the Proregion-VWF paracrystal

Here we show that P-selectin–EGFP is stored in WPBs in an immobile state. Immobility was not directly pH dependent, as P-selectin was immobile in immature (pH 6.2) and mature (pH 5.5) WPBs and in WPBs acutely treated with NH_4Cl (pH>7.4) (Erent et al., 2007). Because P-selectin–EGFP was mostly immobile in pseudo-WPBs of HEK293 cells, it is probable that immobilisation occurs through an interaction with immobile core components in the WPB. The large extracellular domain of P-selectin–EGFP could mediate immobilisation either through a specific interaction with Proregion-VWF tubules or by simply becoming entrapped as the tubules condense into a paracrystal (Berriman et al., 2009). Although the soluble extracellular domain of P-selectin alone is reported to bind the D′-D3 region of VWF (Michaux et al., 2006b), endogenous P-selectin does not bind to VWF in resting HUVECs (Padilla et al., 2004), and does not associate with secreted VWF at the extracellular surface (Babich et al., 2009). Unlike acute exposure to NH_4Cl, where the rod-like WPB morphology (resulting from the Proregion-VWF paracrystal) is retained, prolonged exposure to NH_4Cl causes WPBs to round up and lose their luminal structure (Michaux et al., 2006a), reflecting the disruption of the Proregion-VWF paracrystal. Under these conditions P-selectin–EGFP was mobile, while VWF remained immobile. These data suggest that immobilisation is unlikely to be due to a specific interaction between P-selectin and Proregion or VWF per se, but rather to the presence of the Proregion-VWF paracrystal. Consistent with this is the dramatic slowing of P-selectin release during WPB exocytosis under conditions that prevent complete collapse of the Proregion-VWF paracrystal, as indicated by retention of the rod-like WPB morphology (Babich et al., 2009). Analysis of P-selectin–EGFP mutants in WPBs of HUVECs and HEK293 cells showed that immobilisation depends on the size of the extracellular domain. Taken together these data suggest that immobilisation is due to a steric entrapment of the large extracellular domain of P-selectin by the VWF-Proregion paracrystal.

Immobilisation contributes to P-selectin enrichment in WPBs

WPB exocytosis results in the delivery of P-selectin to the cell surface where it is mobile (Babich et al., 2009) and functions to facilitate attachment and rolling of leukocytes on the vessel wall (Geng et al., 1990). Strong stimulation of WPB exocytosis results in a fourfold increase in P-selectin immunoreactivity at the HUVEC surface (Hattori et al., 1989), indicating that it is present in the WPB membrane at a high concentration. Consistent with this is the striking enrichment of P-selectin in WPBs at the TGN [(Harrison-Lavoie et al., 2006) and Fig. 7A, supplementary material Fig. S3C]. Information for trafficking of P-selectin into WPBs is encoded in the cytoplasmic tail (Blagoveshchenskaya et al., 2002; Disdier et al., 1992; Harrison-Lavoie et al., 2006; Hartwell et al., 1998), although the extracellular domain may also play some role (Harrison-Lavoie et al., 2006). However, a contribution of P-selectin extracellular domain to enrichment of this molecule in WPB membranes has not been reported. Analysis of P-selectin mutants showed that enrichment in immature WPBs at the TGN (Fig. 7A) was associated with immobilisation. Consistent with this, the unrelated membrane protein EGFP–CD63, present and freely mobile in immature and mature WPB membranes showed little evidence of enrichment in WPBs at the TGN. We propose that immobilisation contributes to the retention and enrichment of P-selectin within WPBs. Newly forming WPBs act as sinks in which P-selectin molecules, entering by diffusion through direct membrane connections with the TGN (Harrison-Lavoie et al., 2006; Zenner et al., 2007), become trapped by condensing Proregion-VWF tubules. Truncating the extracellular domain (P-selectin-Δ8CCR–EGFP) prevents entrapment making the diffusional flow of molecules into nascent WPBs reversible, preventing enrichment. In this case the final WPB membrane concentration of P-selectin would not exceed that in the donor TGN membranes.

Materials and Methods

Cell culture and solutions

Primary HUVECs were purchased, cultured, nucleofected and processed for immunocytochemistry as previously described (Babich et al., 2008; Erent et al., 2007; Hannah et al., 2005). For live cell imaging nucleofected cells were plated at

confluent density in culture medium onto 35-mm diameter glass-bottomed culture dishes (MatTeK Corp.) or 25-mm diameter glass coverslips (no. 1.0, 0.15 mm, VWR International, UK). 25-mm diameter glass coverslips were mounted in Rose chambers containing physiological saline (in mM): NaCl 140, KCl 5, $MgSO_4$ 1, $CaCl_2$ 2, glucose 10, HEPES 20, pH 7.3 (adjusted with NaOH). For acute NH_4Cl application 40 mM NaCl was substituted with NH_4Cl, pH 7.3. Experiments were carried out within 45 minutes of exposure to NH_4Cl (typically between 2 and 20 minutes). Complete disruption of WPB morphology was accomplished by preincubation with 40 mM NH_4Cl in culture medium for >3 hours.

At 37°C the extensive mobility of WPBs in HUVECs (Manneville et al., 2003) precluded FRAP experiments, so the whole study was conducted at room temperature 21–23°C at which WPB mobility was reduced. For consistency, cytoplasmic, ER and membrane FRAP studies were also carried out at 21–23°C.

Reagents and immunocytochemistry

Rabbit anti-human VWF was from Dako Ltd (Ely, UK), a sheep anti-human VWF antibody was from Serotec (Kidlington, UK). Polyclonal antibodies specific to the putative C-terminus of human Proregion were raised in rabbit and in chicken (Babich et al., 2009; Giblin et al., 2008). Mouse monoclonal antibody to protein disulphide isomerase (PDI) was from Stressgen (Ann Arbor, MI), mouse monoclonal antibody to Rab27a was from BD Transduction Laboratories (Mississauga, ON). Immunocytochemistry was carried out as previously described (Babich et al., 2009). For PDI staining the cells were fixed in 3% paraformaldehyde with 0.025% glutaraldehyde and pemeabilised with 0.3% Triton X-100 for 5 minutes. For endogenous Rab27a staining cells were fixed in 2% paraformaldehyde and permeabilised with 0.3% Triton X-100 for 5 minutes. Secondary antibodies coupled to fluorophores were from Jackson ImmunoResearch (USA). ProVWF–EGFP, Proregion–EGFP, Proregion–mRFP, tPA–EGFP, P-selectin–EGFP, EGFP–CD63 and eotaxin-3–EGFP were made or obtained as previously described (Babich et al., 2009; Babich et al., 2008; Hannah et al., 2005; Manneville et al., 2003). EGFP–Rab27a and mRFP–Rab27a were constructed using full-length human Rab27a cDNA obtained from the cDNA Resource Center (www.cdna.org). This was cloned into pEGFP–C3 (Clontech) and mRFP–C3 using *Hin*dIII–*Apa*I restriction sites (mRFP–C3 was derived from pEGFP–C3 by exchanging the fluorophores using *Age*I–*Bsr*GI). The signal sequence from rabbit lactase phlorizin hydrolase fused to GFP was cut out of GFP–GL–GPI (Keller et al., 2001) (kindly provided by Kai Simons) and cloned into pEGFP–N1 to produce a soluble secreted form of EGFP (ssEGFP) using *Hin*dIII–*Bsr*GI. P-selectin-ΔCT–EGFP and P-selectin-Δ8CCR–EGFP were made by PCR from full-length P-selectin–EGFP. For P-selectin-ΔCT–EGFP, the cytoplasmic tail (exons 15 and 16) was removed and a *Sal*I site introduced using primers 5′-CAATTCATCTGTGACGAGGG-3′ (forward) and 5′-GCAAAGTCTG-TTTTTCTACTACCCAGCTGATA-3′ (reverse, introducing *Sal*I). The PCR fragment was digested using *Pvu*I and *Sal*I and ligated into *Pvu*I–*Sal*I-digested P-selectin–EGFP. P-selectin-Δ8CCR–EGFP was made by inverse PCR using primers 5′-TGGATATCGTGAAATGCTCAGAACTACATGTTAATAAG-3′ (forward) and 5′-ACGATATCCACGTATTCACATTCTGGCCC-3′ (reverse). The PCR product was self-ligated via an *Eco*RV restriction site. Constructs were sequence verified.

Epifluorescence point-FRAP measurements in the ER

The ER was regarded as an infinite uniform interconnected network of microbranches (Ölveczky and Verkman, 1998) with similar diffusion properties. In such a medium, a focused Gaussian laser beam produces an approximately Gaussian bleach pattern if the illumination duration is short to minimise depletion of the fluorophore (Axelrod et al., 1976; Kiskin and Ogden, 2002). As HUVECs are thin in peripheral regions (<1 μm) compared with the z-axis length of the focused laser spot (1–3 μm), a quasi-cylindrical configuration of the method similar to that used by Yokoe and Meyer (Yokoe and Meyer, 1996) was adopted. The initial concentration of bleached molecules at given radial distance r from the bleaching point is described by the Gaussian function:

$$\frac{B_0}{w_0\sqrt{\pi/2}}\cdot\exp\left[-2r^2/{w_0}^2\right], \quad (1)$$

where the waist of the beam is w_0 and area under the Gaussian B_0. The initial Gaussian bleaching profile remains Gaussian as bleached material redistributes by diffusion in two dimensions in an infinite medium (Jönsson et al., 2008), and the waist w of the above-defined Gaussian expands in time t as:

$$w^2 = {w_0}^2 + 8Dt\,. \quad (2)$$

This allows the quantification of diffusion coefficient D within the ER using two-dimensional averaged radial distributions of bleached fluorophores instead of fluorescence amplitudes, avoiding the deteriorating effects of bleaching and noise inherent to fluorescence amplitude measurements (Jönsson et al., 2008). A Deltavision Imaging System was used: Olympus IX70 inverted microscope, Micromax air-cooled CCD or Cascade2-512 EMCCD (E2V CCD 97B), Olympus U-PLAN-APO 100× 1.35 NA oil immersion objective, QLM FRAP module with a 20 mW 488 nm laser. Laser pulse durations were 10–100 ms, with intensities of 30–100%. EGFP fluorescence was followed using acquisition times of 20–200 ms and 2×2 or higher pixel binning. Image analysis was carried out in the ImageJ software (http://rsb.info.nih.gov/ij; W. S. Rasband, 1997-2010) using custom plugins and macros. Images were digitally smoothed (2×2 mean filter), mean minimal background value was subtracted frame by frame, and five to ten frames before the bleaching were averaged. All recovery frames were subtracted from the averaged prebleach result producing a positive image of the bleached spot spreading radially with time (Fig. 1A-C). The centre of mass of the bleached spot was determined, and the dependences of mean counts on radial distance from the centre constructed for each time frame. The radial distributions were fitted with Gaussians (MathCad 14, MathSoft, USA) and waist values w^2 plotted against time in Origin 7.5 (OriginLab, USA). Values of D were determined from these plots by linear regression using Eqn 2. We defined the percentage of recovery in FRAP as the ratio of the average final fluorescence to the average initial fluorescence in an ~5 μm region surrounding the bleached spot. The depth of bleaching (ratio of minimal fluorescence to initial value) was similar in all experiments, 20–40%.

Confocal FRAP measurements in the WPBs

A Leica TCS SP2 confocal microscope was used with 100× 1.4 NA and 63× 1.32 NA objectives and Leica TCS software in 12-bit bidirectional 'fly' FRAP mode (Leica Microsystems GmbH, Wetzlar, Germany). Electronic zoom was 20–32, confocal pinhole 1.5–2 Airy units and scanning speed 1 kHz. EGFP and mRFP were excited using 488 nm and 561 nm lasers, and emitted light collected at 500-545 and 590-750 nm (EGFP and mRFP imaging, respectively) or 500–650 nm for EGFP in FRAP. For FRAP experiments the long axis of a WPB was aligned horizontally within a rectangular scanning frame, and a horizontal rectangular bleaching region of interest (ROI) defined to cover 20–80% of the WPB length. Laser power within this ROI was increased to 100% during a single bleaching frame, otherwise it was kept at low levels (1–10%). Frame averaging and multiple bleaches were used only for proteins that proved to be immobile or slowly mobile. Images were filtered (2×2 ImageJ mean filter) and background was subtracted.

In confocal FRAP experiments, a 'corona' region extending the bleaching ROI results from the finite dimensions of the bleaching laser beam, fluorophore redistribution during the finite time of bleaching (Kumar et al., 2010) and non-ideal horizontal alignment of WPB. This decreases fluorophore gradients and can lead to underestimation of apparent diffusion coefficients D (Weiss, 2004). Fig. S4A-C in supplementary material shows this corona effect in bleaching of a deposited layer of FITC. Fig. S4D-F in supplementary material shows WPB FRAP evaluation using the linear extension model accounting for the corona effect. For WPB of length L, an initial bleach profile (supplementary material Fig. S4C,E) comprised complete bleaching on the length αL and a linearly decreasing tail extending up to the length βL. We used fluorescence profiles as in supplementary material Fig. S4E to measure this corona extension, $(\beta-\alpha)L$, in each experiment. Values of $(\beta-\alpha)L$ were 0.2–1.1 μm (supplementary material Fig. S4B), similar to those reported previously (Kumar et al., 2010), and were treated here as experimental variables. The position of bleaching ROI in 'fly' mode, the set bleaching proportion α and the length L were taken from image measurements.

A ROI encircling the whole WPB was split into two parts enclosing the bleached [average fluorescence $F1(t)$] and nominally unbleached [average fluorescence $F2(t)$] WPB sections, their length ratio being $\alpha/(1-\alpha)$. These two ROIs were translated and rotated together, tracking WPB motions during FRAP, with fluorescences measured by custom ImageJ plugins. Owing to the extended corona bleaching, at t=0 fluorescence $F2$ exhibited a drop in ΔF from the initial level F_0 [loss of fluorescence in $(\beta-\alpha)L$]. For a uniformly fluorescent close-ended WPB the total amount of fluorescent protein should remain constant, thus the conservation condition:

$$\alpha\times F1(t) + (1-\alpha)\times F2(t) = (F_0-\Delta F)\times(1-\alpha) = const \quad (3)$$

is valid at $t\geq 0$. This equation was used to correct for fluorophore bleaching during recovery and for WPB motion tracking errors. For a completely mobile fluorophore the final steady-state levels $F1(\infty)$ and $F2(\infty)$ should be the same. When recovery was partial, the immobile fraction was quantified as a percent ratio of the difference to the total amount of redistributing fluorescence, $100\%\times[F2(\infty)-F1(\infty)]/F2(0)$. The mobile fraction was defined as 100% minus this value. In experimental traces showing recovery the mobile fraction was near 100%, and small immobile offsets were ignored. Eqn 3 shows that the mean fluorescences $F1(t)$ and $F2(t)$ are linearly dependent records of the recovery kinetics of mobile fluorophore. Thus the decaying $F2(t)$ was inverted, the inversion and component $F1(t)$ were normalised and averaged to improve the signal. The resulting curve was fitted with a diffusional model to find values of D. The model was similar to that in Partikian et al. (Partikian et al., 1998), based on the solution of the diffusion equation for a uniform rod-shaped structure with closed ends and initial profile shown in supplementary material Fig. S4C. We produced a complete solution for the model in a Laplace transform [transform parameter p and the time course $f(p)$] for the normalised bleaching curve:

$$\frac{f(p)}{f_{max}} = \frac{\cosh\left[L(1-\alpha)\sqrt{p/D}\right]-\cosh\left[L(1-\beta)\sqrt{p/D}\right]}{\sinh\left(L\sqrt{p/D}\right)\frac{L^2p^2}{D}\alpha(\beta-\alpha)\left(1-\frac{\alpha+\beta}{2}\right)}\sinh\left(\alpha L\sqrt{p/D}\right), \quad (4)$$

and fitted experimental data by the Levenberg–Marquardt method for D and amplitude (not constrained to 1), using Eqn 4 derivatives for these parameters, with a numerical

inversion of the Laplace transform of this solution. All calculations were performed with Mathcad 14 (MathSoft, USA). We used numerical Laplace inversion methods described by Vlach and Singhal (Vlach and Singhal, 1994) (see Kiskin and Ogden, 2002).

FRAP in the rounded WPB-derived structures

Quantification of protein diffusion on bounded spherical surfaces of rounded-up WPBs was performed using the method of normalised first moment of the membrane fluorescence distribution, according to Cowan et al. and Koppel et al. (Cowan et al., 2004; Koppel et al., 1980). If x is the cosine of equatorial angle θ (Koppel et al., 1980), and the ratio of moments:

$$\mu_1(t) = \int_{-1}^{1} x \cdot C(x,t)\,dx \Big/ \int_{-1}^{1} C(x,t)\,dx \ , \qquad (5)$$

displayed recovery, the result was fitted with decaying exponent $\exp(-t/\tau)$. Diffusion coefficient D was quantified from the τ value and the radius R of rounded WPB (ellipsoid fitted to the image in ImageJ) as:

$$D = R^2/2\tau \ . \qquad (6)$$

The mobile fraction was determined from the peak and steady-state levels of the exponential fit as in Cowan et al. (Cowan et al., 2004).

Data analysis

All results are expressed as mean ± s.e.m., n is the number of cells (ER point-FRAP) or WPBs (confocal FRAP). Statistical significance P-values in nonparametric statistical comparisons were calculated using two-tailed Mann–Whitney test. Statistical calculations were performed in GraphPad Prism 5.02. The critical level of statistical significance was taken as P=0.05.

The relative levels of EGFP in immature WPBs versus adjacent TGN membranes were determined in ImageJ using background-subtracted images of fixed cells triple-stained for EGFP, VWF and the TGN marker TGN46. Grayscale images of all immunofluorescence were synchronised using the Sync Windows plugin (http://rsb.info.nih.gov/ij/plugins/sync-windows.html). Template ROIs were defined to tightly enclose the perimeter of individual immature WPBs using the VWF channel. The same ROIs were synchronously projected on the EGFP image to measure the mean EGFP immunofluorescence within the defined immature WPBs. Mean EGFP immunofluorescences within the TGN were measured from the same WPB template ROIs, shifted to the adjacent TGN46-positive regions lacking VWF staining, according to a colour-merged image of VWF and TGN46 immunoreactivity. The ratios of measurements were compared to avoid expression-dependent bias.

This work was supported by the Medical Research Council, UK. We thank Peter Rosenthal for useful discussions. Deposited in PMC for release after 6 months.

Supplementary material available online at
http://jcs.biologists.org/cgi/content/full/123/17/2964/DC1

References

Arvan, P. and Castle, D. (1998). Sorting and storage during secretory granule biogenesis: looking backward and looking forward. *Biochem. J.* **332**, 593-610.

Axelrod, D., Koppel, D. E., Schlessinger, J., Elson, E. and Webb, W. W. (1976). Mobility measurement by analysis of fluorescence photobleaching recovery kinetics. *Biophys. J.* **16**, 1055-1069.

Babich, V., Meli, A., Knipe, L., Dempster, J. E., Skehel, P., Hannah, M. J. and Carter, T. (2008). Selective release of molecules from Weibel Palade bodies during a lingering kiss. *Blood* **111**, 5282-5290.

Babich, V., Knipe, L., Hewlett, L., Meli, A., Dempster, J., Hannah, M. J. and Carter, T. (2009). Differential effect of extracellular acidosis on the release and dispersal of soluble and membrane proteins secreted from the Weibel-Palade body. *J. Biol. Chem.* **284**, 12459-12468.

Berriman, J. A., Li, S., Hewlett, L. J., Wasilewski, S., Kiskin, F. N., Carter, T., Hannah, M. J. and Rosenthal, P. B. (2009). Structural organization of Weibel-Palade bodies revealed by cryo-EM of vitrified endothelial cells. *Proc. Natl. Acad. Sci. USA* **106**, 17407-17412.

Blagoveshchenskaya, A. D., Hannah, M. J., Allen, S. and Cutler, D. F. (2002). Selective and signal-dependent recruitment of membrane proteins to secretory granules formed by heterologously expressed von Willebrand factor. *Mol. Biol. Cell* **13**, 1582-1593.

Cowan, A. E., Olivastro, E. M., Koppel, D. E., Loshon, C. A., Setlow, B. and Setlow, P. (2004). Lipids in the inner membrane of dormant spores of Bacillus species are largely immobile. *Proc. Natl. Acad. Sci. USA* **101**, 7733-7738.

Dayel, M. J., Hom, E. F. and Verkman, A. S. (1999). Diffusion of green fluorescent protein in the aqueous-phase lumen of endoplasmic reticulum. *Biophys. J.* **76**, 2843-2851.

Disdier, M., Morrissey, J. H., Fugate, R. D., Bainton, D. F. and McEver, R. P. (1992). Cytoplasmic domain of P-selectin (CD62) contains the signal for sorting into the regulated secretory pathway. *Mol. Biol. Cell* **3**, 309-321.

Dross, N., Spriet, C., Zwerger, M., Muller, G., Waldeck, W. and Langowski, J. (2009). Mapping eGFP oligomer mobility in living cell nuclei. *PLoS ONE* **4**, e5041.

Ellgaard, L. and Helenius, A. (2003). Quality control in the endoplasmic reticulum. *Nat. Rev. Mol. Cell Biol.* **4**, 181-191.

Erent, M., Meli, A., Moisoi, N., Babich, V., Hannah, M. J., Skehel, P., Knipe, L., Zupancic, G., Ogden, D. and Carter, T. D. (2007). Rate, extent and concentration-dependence of histamine-evoked Weibel-Palade body exocytosis determined from individual fusion events in human endothelial cells. *J. Physiol.* **583**, 195-212.

Ewenstein, B. M., Warhol, M. J., Handin, R. I. and Pober, J. S. (1987). Composition of the von Willebrand factor storage organelle (Weibel-Palade body) isolated from cultured human umbilical vein endothelial cells. *J. Cell Biol.* **104**, 1423-1433.

Geng, J. G., Bevilacqua, M. P., Moore, K. L., McIntyre, T. M., Prescott, S. M., Kim, J. M., Bliss, G. A., Zimmerman, G. A. and McEver, R. P. (1990). Rapid neutrophil adhesion to activated endothelium mediated by GMP-140. *Nature* **343**, 757-760.

Giblin, J. P., Hewlett, L. J. and Hannah, M. J. (2008). Basal secretion of von Willebrand factor from human endothelial cells. *Blood* **112**, 957-964.

Hannah, M. J., Williams, R., Kaur, J., Hewlett, L. J. and Cutler, D. F. (2002). Biogenesis of Weibel-Palade bodies. *Semin. Cell Dev. Biol.* **13**, 313-324.

Hannah, M. J., Hume, A. N., Arribas, M., Williams, R., Hewlett, L. J., Seabra, M. C. and Cutler, D. F. (2003). Weibel-Palade bodies recruit Rab27 by a content-driven, maturation-dependent mechanism that is independent of cell type. *J. Cell Sci.* **116**, 3939-3948.

Hannah, M. J., Skehel, P., Erent, M., Knipe, L., Ogden, D. and Carter, T. (2005). Differential kinetics of cell surface loss of von Willebrand factor and its propolypeptide after secretion from Weibel-Palade bodies in living human endothelial cells. *J. Biol. Chem.* **280**, 22827-22830.

Harrison-Lavoie, K. J., Michaux, G., Hewlett, L., Kaur, J., Hannah, M. J., Lui-Roberts, W. W., Norman, K. E. and Cutler, D. F. (2006). P-selectin and CD63 use different mechanisms for delivery to Weibel-Palade bodies. *Traffic* **7**, 647-662.

Hartwell, D. W., Mayadas, T. N., Berger, G., Frenette, P. S., Rayburn, H., Hynes, R. O. and Wagner, D. D. (1998). Role of P-selectin cytoplasmic domain in granular targeting in vivo and in early inflammatory responses. *J. Cell Biol.* **143**, 1129-1141.

Hattori, R., Hamilton, K. K., Fugate, R. D., McEver, R. P. and Sims, P. J. (1989). Stimulated secretion of endothelial von Willebrand factor is accompanied by rapid redistribution to the cell surface of the intracellular granule membrane protein GMP-140. *J. Biol. Chem.* **264**, 7768-7771.

Hemler, M. E. (2005). Tetraspanin functions and associated microdomains. *Nat. Rev. Mol. Cell Biol.* **6**, 801-811.

Jackson, C. L. (2009). Mechanisms of transport through the Golgi complex. *J. Cell Sci.* **122**, 443-452.

Jönsson, P., Jonsson, M. P., Tegenfeldt, J. O. and Hook, F. (2008). A method improving the accuracy of fluorescence recovery after photobleaching analysis. *Biophys. J.* **95**, 5334-5348.

Kao, H. P., Abney, J. R. and Verkman, A. S. (1993). Determinants of the translational mobility of a small solute in cell cytoplasm. *J. Cell Biol.* **120**, 175-184.

Katsumata, O., Fujita-Yoshigaki, J., Hara-Yokoyama, M., Yanagishita, M., Furuyama, S. and Sugiya, H. (2007). Syntaxin6 separates from GM1a-rich membrane microdomain during granule maturation. *Biochem. Biophys. Res. Commun.* **357**, 1071-1077.

Keller, P., Toomre, D., Diaz, E., White, J. and Simons, K. (2001). Multicolour imaging of post-Golgi sorting and trafficking in live cells. *Nat. Cell Biol.* **3**, 140-149.

Kiskin, N. I. and Ogden, D. (2002). Two-photon excitation and photolysis by pulsed laser illumination modelled by spatially non-uniform reactions with simultaneous diffusion. *Eur. Biophys. J.* **30**, 571-587.

Klumperman, J., Kuliawat, R., Griffith, J. M., Geuze, H. J. and Arvan, P. (1998). Mannose 6-phosphate receptors are sorted from immature secretory granules via adaptor protein AP-1, clathrin, and syntaxin 6-positive vesicles. *J. Cell Biol.* **141**, 359-371.

Koppel, D. E., Sheetz, M. P. and Schindler, M. (1980). Lateral diffusion in biological membranes. A normal-mode analysis of diffusion on a spherical surface. *Biophys. J.* **30**, 187-192.

Kumar, M., Mommer, M. S. and Sourjik, V. (2010). Mobility of cytoplasmic, membrane, and DNA-binding proteins in Escherichia coli. *Biophys. J.* **98**, 552-559.

Lippincott-Schwartz, J., Roberts, T. H. and Hirschberg, K. (2000). Secretory protein trafficking and organelle dynamics in living cells. *Annu. Rev. Cell Dev. Biol.* **16**, 557-589.

Lui-Roberts, W. W., Collinson, L. M., Hewlett, L. J., Michaux, G. and Cutler, D. F. (2005). An AP-1/clathrin coat plays a novel and essential role in forming the Weibel-Palade bodies of endothelial cells. *J. Cell Biol.* **170**, 627-636.

Lukacs, G. L., Haggie, P., Seksek, O., Lechardeur, D., Freedman, N. and Verkman, A. S. (2000). Size-dependent DNA mobility in cytoplasm and nucleus. *J. Biol. Chem.* **275**, 1625-1629.

Manneville, J. B., Etienne-Manneville, S., Skehel, P., Carter, T., Ogden, D. and Ferenczi, M. (2003). Interaction of the actin cytoskeleton with microtubules regulates secretory organelle movement near the plasma membrane in human endothelial cells. *J. Cell Sci.* **116**, 3927-3938.

Michaux, G., Abbitt, K. B., Collinson, L. M., Haberichter, S. L., Norman, K. E. and Cutler, D. F. (2006a). The physiological function of von Willebrand's factor depends on its tubular storage in endothelial Weibel-Palade bodies. *Dev. Cell* **10**, 223-232.

Michaux, G., Pullen, T. J., Haberichter, S. L. and Cutler, D. F. (2006b). P-selectin binds to the D′-D3 domains of von Willebrand factor in Weibel-Palade bodies. *Blood* **107**, 3922-3924.

Nagaya, H., Tamura, T., Higa-Nishiyama, A., Ohashi, K., Takeuchi, M., Hashimoto, H., Hatsuzawa, K., Kinjo, M., Okada, T. and Wada, I. (2008). Regulated motion of

glycoproteins revealed by direct visualization of a single cargo in the endoplasmic reticulum. *J. Cell Biol.* **180**, 129-143.

Novak, I. L., Kraikivski, P. and Slepchenko, B. M. (2009). Diffusion in cytoplasm: effects of excluded volume due to internal membranes and cytoskeletal structures. *Biophys. J.* **97**, 758-767.

Ölveczky, B. P. and Verkman, A. S. (1998). Monte Carlo analysis of obstructed diffusion in three dimensions: application to molecular diffusion in organelles. *Biophys. J.* **74**, 2722-2730.

Padilla, A., Moake, J. L., Bernardo, A., Ball, C., Wang, Y., Arya, M., Nolasco, L., Turner, N., Berndt, M. C., Anvari, B. et al. (2004). P-selectin anchors newly released ultralarge von Willebrand factor multimers to the endothelial cell surface. *Blood* **103**, 2150-2156.

Papadopoulos, S., Jurgens, K. D. and Gros, G. (2000). Protein diffusion in living skeletal muscle fibers: dependence on protein size, fiber type, and contraction. *Biophys. J.* **79**, 2084-2094.

Partikian, A., Olveczky, B., Swaminathan, R., Li, Y. and Verkman, A. S. (1998). Rapid diffusion of green fluorescent protein in the mitochondrial matrix. *J. Cell Biol.* **140**, 821-829.

Pereira-Leal, J. B., Hume, A. N. and Seabra, M. C. (2001). Prenylation of Rab GTPases: molecular mechanisms and involvement in genetic disease. *FEBS Lett.* **498**, 197-200.

Perez-Vilar, J., Mabolo, R., McVaugh, C. T., Bertozzi, C. R. and Boucher, R. C. (2006). Mucin granule intraluminal organization in living mucous/goblet cells. Roles of protein post-translational modifications and secretion. *J. Biol. Chem.* **281**, 4844-4855.

Pols, M. S. and Klumperman, J. (2009). Trafficking and function of the tetraspanin CD63. *Exp. Cell Res.* **315**, 1584-1592.

Poole, B. and Ohkuma, S. (1981). Effect of weak bases on the intralysosomal pH in mouse peritoneal macrophages. *J. Cell Biol.* **90**, 665-669.

Purvis, A. R., Gross, J., Dang, L. T., Huang, R. H., Kapadia, M., Townsend, R. R. and Sadler, J. E. (2007). Two Cys residues essential for von Willebrand factor multimer assembly in the Golgi. *Proc. Natl. Acad. Sci. USA* **104**, 15647-15652.

Roos, A. and Boron, W. F. (1981). Intracellular pH. *Physiol. Rev.* **61**, 296-434.

Seksek, O., Biwersi, J. and Verkman, A. S. (1997). Translational diffusion of macromolecule-sized solutes in cytoplasm and nucleus. *J. Cell Biol.* **138**, 131-142.

Singh, I., Shankaran, H., Beauharnois, M. E., Xiao, Z., Alexandridis, P. and Neelamegham, S. (2006). Solution structure of human von Willebrand factor studied using small angle neutron scattering. *J. Biol. Chem.* **281**, 38266-38275.

Snapp, E. L., Sharma, A., Lippincott-Schwartz, J. and Hegde, R. S. (2006). Monitoring chaperone engagement of substrates in the endoplasmic reticulum of live cells. *Proc. Natl. Acad. Sci. USA* **103**, 6536-6541.

Swaminathan, R., Hoang, C. P. and Verkman, A. S. (1997). Photobleaching recovery and anisotropy decay of green fluorescent protein GFP-S65T in solution and cells: cytoplasmic viscosity probed by green fluorescent protein translational and rotational diffusion. *Biophys. J.* **72**, 1900-1907.

Tooze, S. A., Martens, G. J. and Huttner, W. B. (2001). Secretory granule biogenesis: rafting to the SNARE. *Trends Cell. Biol.* **11**, 116-122.

Valentijn, K. M., Valentijn, J. A., Jansen, K. A. and Koster, A. J. (2008). A new look at Weibel-Palade body structure in endothelial cells using electron tomography. *J. Struct. Biol.* **161**, 447-458.

Verkman, A. S. (2002). Solute and macromolecule diffusion in cellular aqueous compartments. *Trends Biochem. Sci.* **27**, 27-33.

Vlach, J. and Singhal, K. (1994). Numerical Laplace transform inversion. In *Computer Methods for Circle Analysis and Design* (ed. J. Vlach), pp. 349-390. New York: Van Nostrand Reinhold.

Weibel, E. R. and Palade, G. E. (1964). New cytoplasmic components in arterial endothelia. *J. Cell Biol.* **23**, 101-112.

Weiss, M. (2004). Challenges and artifacts in quantitative photobleaching experiments. *Traffic* **5**, 662-671.

Yokoe, H. and Meyer, T. (1996). Spatial dynamics of GFP-tagged proteins investigated by local fluorescence enhancement. *Nat. Biotechnol.* **14**, 1252-1256.

Zenner, H. L., Collinson, L. M., Michaux, G. and Cutler, D. F. (2007). High-pressure freezing provides insights into Weibel-Palade body biogenesis. *J. Cell Sci.* **120**, 2117-2125.